

Publication VIII

Piippo, A., Suomela, K., Hinkkanen, M., and Luomi, J. (2007). "Sensorless PMSM drive with DC-link current measurement." In *Conference Record of the 42nd IEEE-Industry Applications Society (IAS) Annual Meeting*, pp. 2371–2377, New Orleans, LA.

© 2007 IEEE. Reprinted with permission.

This material is posted here with permission of the IEEE. Such permission of the IEEE does not in any way imply IEEE endorsement of any of the Helsinki University of Technology's products or services. Internal or personal use of this material is permitted. However, permission to reprint/republish this material for advertising or promotional purposes or for creating new collective works for resale or redistribution must be obtained from the IEEE by writing to pubs-permissions@ieee.org.

By choosing to view this material, you agree to all provisions of the copyright laws protecting it.

Sensorless PMSM Drive With DC-Link Current Measurement

Antti Piippo*, Kalle Suomela[†], Marko Hinkkanen*, and Jorma Luomi*

*Helsinki University of Technology
Power Electronics Laboratory
P.O. Box 3000, FI-02015 TKK, Finland

[†]ABB Oy
Drives
P.O. Box 184, FI-00381 Helsinki, Finland

Abstract—The paper proposes a motion-sensorless control method for permanent magnet synchronous motor drives when only the DC-link current is measured instead of the motor phase currents. A two-phase pulse-width modulation method is used, allowing the DC-link current to be sampled twice in a switching period at uniform intervals during active voltage vectors. A method is proposed for obtaining the current feedback for vector control, and an adaptive observer is used for estimating the rotor speed and position. The estimation is augmented with a high-frequency signal injection method at low speeds; a modified high-frequency excitation voltage is proposed for better performance. The proposed method enables stable operation of the permanent magnet synchronous motor drive in a wide speed range and under various loads. The effectiveness of the proposed method is demonstrated both by simulations and laboratory experiments.

I. INTRODUCTION

Vector control of AC motors requires feedback from the phase currents of the motor. Usually, these currents are obtained by measuring at least two of the phase currents. The phase currents have to be measured by devices that are electrically isolated from the control electronics. Hall-effect sensors, commonly used for this purpose, are expensive components in low-cost frequency converters. In addition, deviations in the gains between the current sensors of different phases can cause current ripple and, consequently, torque ripple. A cost-effective alternative to the phase current measurement is to measure the DC-link current of the frequency converter [1]. If vector control is employed, the phase currents of the motor can be estimated using the DC-link current and the information on the states of the inverter switches.

Previously, various methods have been proposed for the estimation of the phase currents when only the DC-link current is measured. Exclusively nonzero voltage vectors have been used in a direct torque controlled induction motor drive [2]. A state observer has been applied for providing the stator current feedback of a permanent magnet synchronous motor (PMSM), updating the phase currents from the available samples during every three-phase pulse-width modulation (PWM) cycle [3]. Multiple samples can be taken in every switching period of the three-phase PWM to obtain the phase currents [4]. A model has been developed for extracting instantaneous active and reactive power information from the DC-link current [5]. Discrete voltage vectors used for sensorless position detection have also been used in combination with the DC-link current measurement at low speeds—space-vector PWM being applied at higher speeds [6]. Phase currents can also be sampled during active voltage vectors applied in an additional excitation

voltage sequence [7].

Some of the previous methods require modifications in the inverter switching pattern [2], [7], which causes increased voltage and current distortion and additional losses. The methods in [3], [4], [6] are based on three-phase PWM and require non-uniform sampling (i.e. variable sampling intervals) to detect the phase currents. Faster A/D conversion and signal processing are needed as compared with uniform sampling. Furthermore, it is desired to obtain the fundamental current—and to reject the switching frequency and its harmonics—by appropriate sampling in vector control. Usually, sampling synchronized to the modulation is used for this purpose. When non-uniform sampling is applied, the benefit of rejecting the switching frequency by the synchronized sampling is lost, and additional compensation algorithms have to be used. The method proposed in [4] requires four current samples in each switching period to reject the current ripple caused by the inverter.

This paper deals with a sensorless PMSM drive equipped with a single current sensor in the DC link. A two-phase (discontinuous) PWM method [8]–[10] is used, and the DC-link current is sampled at uniform intervals in the beginning and in the center of the switching periods [11]. In two-phase modulation, one of the inverter output phases stays in the negative or in the positive DC bus and the two other phases are modulated to create the desired phase-to-phase voltage. A method for obtaining the current feedback is proposed, based on the current estimation error in the estimated rotor reference frame. An adaptive observer [12] is used for the rotor speed and position estimation, and for estimating the stator current. A high-frequency (HF) signal injection method is used at low speeds to stabilize the estimation; a modified HF excitation voltage is proposed for obtaining phase current samples regularly. The performance of the proposed method is investigated by means of simulations, and experimental results obtained with a low-cost frequency converter are presented.

II. PMSM MODEL

The PMSM is modeled in the d - q reference frame fixed to the rotor. The d axis is oriented along the permanent magnet flux, whose angle in the stator reference frame is θ_m in electrical radians. The stator voltage equation is

$$\mathbf{u}_s = R_s \mathbf{i}_s + \dot{\boldsymbol{\psi}}_s + \omega_m \mathbf{J} \boldsymbol{\psi}_s \quad (1)$$

where $\mathbf{u}_s = [u_d \ u_q]^T$ is the stator voltage, $\mathbf{i}_s = [i_d \ i_q]^T$ the stator current, $\boldsymbol{\psi}_s = [\psi_d \ \psi_q]^T$ the stator flux, R_s the stator

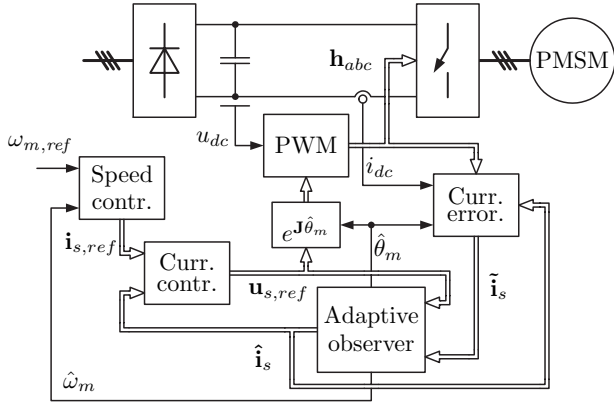


Fig. 1. Block diagram of the control system. Block “Speed contr.” includes both the speed controller and the calculation of the current reference.

resistance, $\omega_m = \dot{\theta}_m$ the electrical angular speed of the rotor, and

$$\mathbf{J} = \begin{bmatrix} 0 & -1 \\ 1 & 0 \end{bmatrix}$$

The stator flux is

$$\boldsymbol{\psi}_s = \mathbf{L}\mathbf{i}_s + \boldsymbol{\psi}_{pm} \quad (2)$$

where $\boldsymbol{\psi}_{pm} = [\psi_{pm} \ 0]^T$ is the permanent magnet flux and

$$\mathbf{L} = \begin{bmatrix} L_d & 0 \\ 0 & L_q \end{bmatrix}$$

is the inductance matrix, L_d and L_q being the direct- and quadrature-axis inductances, respectively. The electromagnetic torque is given by

$$T_e = \frac{3p}{2} \boldsymbol{\psi}_s^T \mathbf{J}^T \mathbf{i}_s \quad (3)$$

where p is the number of pole pairs.

III. PWM AND CURRENT FEEDBACK

Fig. 1 shows the block diagram of the control system comprising cascaded speed and current control loops. The only measured quantities are the DC-link voltage u_{dc} and the DC-link current i_{dc} at the input of the inverter. The estimated electrical angular speed and position of the rotor are denoted by $\hat{\omega}_m$ and $\hat{\theta}_m$, respectively. The current estimation error $\tilde{\mathbf{i}}_s$ is calculated using the estimated current $\hat{\mathbf{i}}_s$, the DC-link current i_{dc} , and the knowledge of the inverter switching states \mathbf{h}_{abc} . This current error is used for feedback in an adaptive observer described in Section IV.

The three-phase voltage-source inverter has eight discrete switching states. Six active inverter states produce nonzero phase-to-phase voltages to the three-phase load, and the two remaining states produce zero output voltages. The DC-link current is nonzero only during active inverter states; it has to be sampled during an active state for obtaining information on phase currents.

The DC-link current equals one of the phase currents (i_a , i_b , or i_c) at a time, depending on the inverter switching state. The relation between the inverter switching states $\mathbf{h}_{abc} =$

TABLE I
DC-LINK CURRENT DEPENDENCE ON THE INVERTER SWITCHING STATES

h_a	h_b	h_c	i_{dc}
0	0	0	–
1	0	0	i_a
1	1	0	$-i_c$
0	1	0	i_b
0	1	1	$-i_a$
0	0	1	i_c
1	0	1	$-i_b$
1	1	1	–

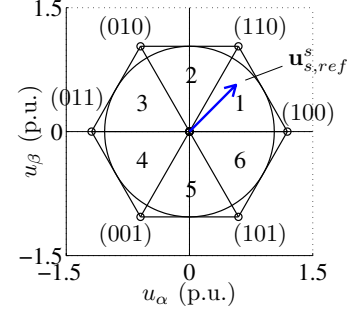


Fig. 2. Nonzero output voltage vectors and stator voltage reference vector $\mathbf{u}_{s,ref}^s$ in stationary reference frame. The switching states and the sector numbers are also shown.

$[h_a \ h_b \ h_c]$ and the phase current obtainable from the DC-link current i_{dc} is given in Table I. The switching state h of each phase equals either 0 or 1, corresponding to the inverter output phase switched to the negative or positive DC bus, respectively. The nonzero output voltage vectors divide the voltage plane into six sectors as illustrated in Fig. 2. The magnitudes of the active voltage vectors equal $\frac{2}{3}u_{dc}$.

A. Two-Phase PWM

Two-phase modulation [8] is selected as the PWM method. As compared to three-phase PWM, the two-phase PWM has an advantage of reduced switching losses. For each sampling period, the durations of the two active voltage vectors to be applied to the motor are calculated. The zero voltage vector can be chosen arbitrarily without affecting the phase-to-phase voltages of the motor. In two-phase PWM methods, the zero vectors can be applied either at the beginning and at the end of the switching period, or at the center of the switching period. Usually, the zero voltage vector is changed at the sector boundaries: in [9], the upper zero voltage vector (all phases connected to the positive DC bus) was used in the odd sectors, whereas the lower zero voltage vector (all phases connected to the negative DC bus) was used in the odd sectors in [10]. Correspondingly, the lower and the upper zero voltage vectors were used in the even sectors in [9] and [10], respectively. Here, these two methods are alternated at regular intervals [11].

The switching states resulting from the voltage reference vector depicted in Fig. 2 are shown in Fig. 3 for one switching period $2T_s$, T_s being the length of the sampling period. The results of three-phase space vector modulation [Fig. 3(a)] and two-phase vector modulation with lower [Fig. 3(b)] and

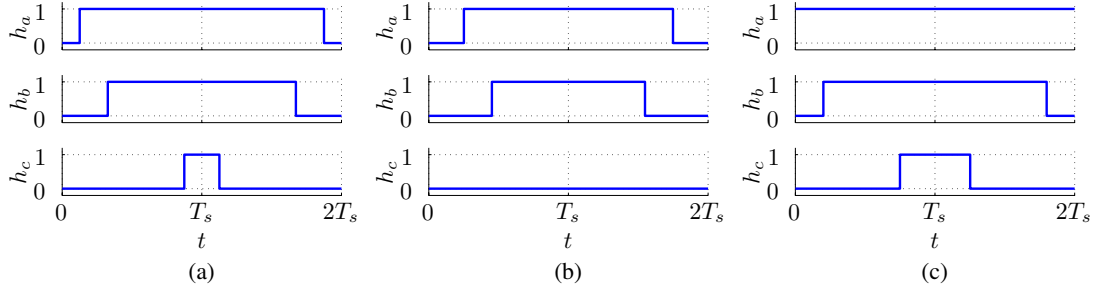


Fig. 3. Switching states corresponding to the voltage reference in Fig. 2 during one switching period: (a) three-phase space-vector modulation; (b) two-phase modulation with lower zero voltage vector; (c) two-phase modulation with upper zero voltage vector. The time instants $t = 0$ and $t = T_s$ are referred to as the beginning and the center of the switching period, respectively.

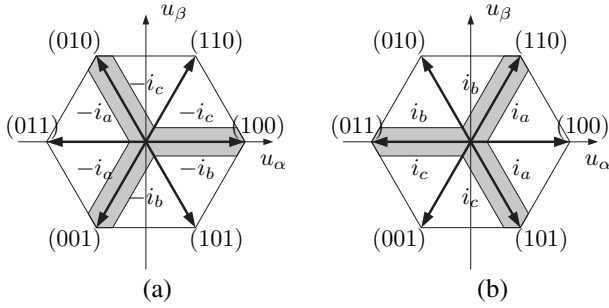


Fig. 4. Phase current corresponding to the DC-link current for voltage reference in different sectors of the stator reference frame: (a) lower zero voltage vector (000); (b) upper zero voltage vector (111). The unallowable regions due to the minimum pulse limitation are shown as gray areas.

upper [Fig. 3(c)] zero vectors are shown for the same voltage reference. All the three methods produce the same average phase-to-phase voltages. With the lower zero voltage vector, the active voltage vectors are applied in the center of the switching period, whereas with the upper zero voltage vector, the active voltage vectors are applied in the beginning and in the end of the period.

B. Current Feedback

The DC-link current is sampled uniformly in the beginning and in the center of the switching period in a fashion similar to [11]. One of the two current samples is obtained during an active voltage vector, and this sample corresponds to one of the phase currents. Thus one phase current can be determined by using the known switching state references and the information given in Table I. The phase current available in each voltage sector is shown in Fig. 4 for both lower and upper zero voltage vectors. In each sector, two phase currents can be obtained by changing the zero vector. The third phase current cannot be sampled until the voltage reference vector crosses a sector border.

In the control system, the observer presented in Section IV provides the estimated stator current $\hat{\mathbf{i}}_s$, and the feedback in the observer is based on the current estimation error $\tilde{\mathbf{i}}_s$. The estimation error is updated using the phase current samples when possible, and kept constant if samples are not obtained. For updating the estimation error, the estimated stator current

$\hat{\mathbf{i}}_s$ and the current error $\tilde{\mathbf{i}}_s$ are transformed to phase quantities in the stationary reference frame, i.e.

$$\hat{\mathbf{i}}_{abc} = \mathbf{T}_{abc} \hat{\mathbf{i}}_s \quad (4)$$

$$\tilde{\mathbf{i}}_{abc} = \mathbf{T}_{abc} \tilde{\mathbf{i}}_s \quad (5)$$

where

$$\mathbf{T}_{abc} = \begin{bmatrix} \cos(\hat{\theta}_m) & -\sin(\hat{\theta}_m) \\ \cos(\hat{\theta}_m - \frac{2\pi}{3}) & -\sin(\hat{\theta}_m - \frac{2\pi}{3}) \\ \cos(\hat{\theta}_m + \frac{2\pi}{3}) & -\sin(\hat{\theta}_m + \frac{2\pi}{3}) \end{bmatrix} \quad (6)$$

is the transformation matrix from the estimated rotor reference frame to the phase quantities. The current error $\tilde{\mathbf{i}}_{abc} = [\tilde{i}_a \ \tilde{i}_b \ \tilde{i}_c]^T$ is updated if a phase current sample is available. If the current i_a of the phase a is available, for example, the current estimation error is updated using

$$\tilde{i}_a = i_a - \hat{i}_a \quad (7)$$

After updating, the current error is transformed back to the estimated rotor reference frame using

$$\tilde{\mathbf{i}}_s = \mathbf{T}_{dq} \tilde{\mathbf{i}}_{abc} \quad (8)$$

where

$$\mathbf{T}_{dq} = \frac{2}{3} \begin{bmatrix} \cos(-\hat{\theta}_m) & \sin(-\hat{\theta}_m) \\ \cos(-\hat{\theta}_m + \frac{2\pi}{3}) & \sin(-\hat{\theta}_m + \frac{2\pi}{3}) \\ \cos(-\hat{\theta}_m - \frac{2\pi}{3}) & \sin(-\hat{\theta}_m - \frac{2\pi}{3}) \end{bmatrix}^T \quad (9)$$

is the transformation matrix from the phase quantities to the estimated rotor reference frame. The operations described above are executed during every sampling period, i.e. at intervals of T_s .

The estimated current is used as feedback in the current controller. However, the stator current can be reconstructed from the estimated current and the current error by

$$\mathbf{i}_{s,dc} = \hat{\mathbf{i}}_s + \tilde{\mathbf{i}}_s \quad (10)$$

When this reconstructed current is used in the integral part of the current controller, the steady-state error caused by parameter errors in the current control can be avoided.

C. Minimum Pulse Limitation

The high rate of change of the inverter output voltage (i.e. high du/dt) during switching causes transients in the voltages and currents of the inverter output phases. These transients disturb the current measurement during short inverter voltage pulses, and reliable current samples cannot be obtained shortly after switching. To improve the current measurement, the minimum duration of the voltage pulse, during which the current is sampled, has to be lengthened. Consequently, short active voltage vectors cannot be used in the beginning and in the center of the switching period. The effect of the minimum pulse limitation on the allowable stator voltage vector is depicted in Fig. 4 for both lower and upper zero vectors.

The minimum pulse limitation distorts the stator voltage, especially at low stator voltage values (i.e. at low modulation index values). The estimation errors of the stator current, rotor speed, and rotor position caused by the voltage distortion are reduced by using the realizable (distorted) stator voltage in the adaptive observer described in Section IV.

IV. OBSERVER

A. Adaptive Observer

An adaptive observer [12] is used for the estimation of the stator current, rotor speed, and rotor position. The speed and position estimation is based on the estimation error between two different models; the actual motor can be considered as a reference model and the observer—including the rotor speed estimate $\hat{\omega}_m$ —as an adjustable model. An error term used in an adaptation mechanism is based on the estimation error of the stator current. The estimated rotor speed, obtained by the adaptation mechanism, is fed back to the adjustable model.

The adaptive observer is formulated in the estimated rotor reference frame. The stator flux is selected as a state variable in the adjustable model,

$$\dot{\hat{\psi}}_s = \mathbf{u}_{s,ref} - \hat{R}_s \hat{\mathbf{i}}_s - \hat{\omega}_m \mathbf{J} \hat{\psi}_s + \boldsymbol{\lambda} \tilde{\mathbf{i}}_s \quad (11)$$

where estimated quantities are marked by $\hat{\cdot}$ and $\mathbf{u}_{s,ref}$ is the stator voltage reference. The estimate of the stator current is

$$\hat{\mathbf{i}}_s = \hat{\mathbf{L}}^{-1}(\hat{\psi}_s - \hat{\psi}_{pm}) \quad (12)$$

The current error is calculated based on available current samples as described in Section III-B. The feedback gain matrix $\boldsymbol{\lambda}$ is varied as a function of the rotor speed [12].

The adaptation is based on an error term

$$F_\varepsilon = [0 \quad L_q] \tilde{\mathbf{i}}_s \quad (13)$$

i.e. the current error in the estimated q direction is used for adaptation. The estimate of the electrical angular speed of the rotor is obtained by a PI speed adaptation mechanism

$$\dot{\hat{\omega}}_m = -k_p F_\varepsilon - k_i \int F_\varepsilon dt \quad (14)$$

where k_p and k_i are nonnegative gains. The estimate $\hat{\theta}_m$ for the rotor position is obtained by integrating $\hat{\omega}_m$.

B. High-Frequency Signal Injection

Since the adaptive observer cannot perform well at low speeds due to inaccuracies in measurements and parameter estimates, an HF signal injection method is used to stabilize the observer [13]. Originally, a carrier excitation signal alternating on the d axis at angular frequency ω_c and having an amplitude u_c , i.e.

$$\mathbf{u}_{c1} = u_c \begin{bmatrix} \cos(\omega_c t) \\ 0 \end{bmatrix} \quad (15)$$

is superimposed on the voltage reference in the estimated rotor reference frame. An alternating current response is detected on the q axis of the estimated rotor reference frame, amplitude modulated by the rotor position estimation error $\hat{\theta}_m = \theta_m - \hat{\theta}_m$. Demodulation and low-pass filtering results in an error signal ε that is approximately proportional to $\hat{\theta}_m$.

At low speeds and standstill, the stator voltage reference can move between sectors too slowly for detecting all phase currents regularly. Although the HF excitation voltage in (15) results in varying voltage reference, different sectors may not be covered equally enough. Consequently, one of the stator phase currents may be unavailable for a long period, and the signal injection cannot detect the rotor position reliably. For better sector coverage, a modified HF excitation voltage

$$\mathbf{u}_{c2} = u_c \begin{bmatrix} \cos(\omega_c t) \\ \sin(2\omega_c t) \end{bmatrix} \quad (16)$$

is proposed. Thus, the second harmonic of the excitation frequency is injected to the q axis of the estimated rotor reference frame. The second harmonic appears in the stator current, but it does not affect the error signal ε since the demodulation is only sensitive to frequency ω_c .

The error signal ε is used for correcting the estimated position by influencing the direction of the stator flux estimate of the adjustable model. The algorithm is given by

$$\dot{\hat{\psi}}_{s,u} = \mathbf{u}_{s,ref} - \hat{R}_s \hat{\mathbf{i}}_s - (\hat{\omega}_m - \omega_\varepsilon) \mathbf{J} \hat{\psi}_{s,u} + \boldsymbol{\lambda} \tilde{\mathbf{i}}_s \quad (17)$$

and

$$\omega_\varepsilon = \gamma_p \varepsilon + \gamma_i \int \varepsilon dt \quad (18)$$

where γ_p and γ_i are the nonnegative gains of the PI mechanism driving the error signal ε to zero. At low speeds, both the signal injection method and the adaptive observer contribute to the rotor speed and position estimation. The influence of the HF signal injection is decreased linearly with increasing speed, reaching zero at a certain speed [13]. At higher speeds, the estimation is based only on the adaptive observer.

It is important that the HF excitation voltage in (16) is included in the voltage reference fed to the adjustable model in (17). The HF excitation voltage ensures reliable prediction of the HF current in the stator current estimate $\hat{\mathbf{i}}_s$, which is needed for calculating the current error. It is to be noted that the reconstructed stator current $\hat{\mathbf{i}}_{s,dc}$ (10) has to be used for demodulation in the signal injection method instead of the estimated current $\hat{\mathbf{i}}_s$.

TABLE II
MOTOR DATA

Nominal power	2.2 kW
Nominal voltage U_N	370 V
Nominal current I_N	4.3 A
Nominal frequency f_N	75 Hz
Nominal speed	1 500 r/min
Nominal torque T_N	14.0 Nm
Number of pole pairs p	3
Stator resistance R_s	3.59 Ω
Direct-axis inductance L_d	0.036 H
Quadrature-axis inductance L_q	0.051 H
Permanent magnet flux ψ_{pm}	0.545 Vs
Total moment of inertia	0.015 kgm ²

V. SIMULATION RESULTS

The proposed method was investigated by means of simulations and laboratory experiments. Fig. 1 shows the block diagram of the control system comprising cascaded speed and current control loops. PI-type speed control with active damping is used. The current reference $i_{s,ref}$ is calculated according to maximum torque per current control. The current control is implemented as PI-type control in the estimated rotor reference frame.

The data of the six-pole interior-magnet PMSM (2.2 kW, 1500 rpm) are given in Table II. The base values for voltage, current, and angular speed are defined as $\sqrt{2/3}U_N$, $\sqrt{2}I_N$, and $2\pi f_N$, respectively. The electromagnetic torque is limited to 22 Nm, which is 1.57 times the nominal torque T_N . The high-frequency carrier excitation signal has a frequency of 500 Hz and an amplitude of 90 V. The HF signal injection is used below the speed of 0.13 p.u. The speed control and current control bandwidths are 5 Hz and 200 Hz, respectively. The observer parameters were selected as in [12].

The MATLAB/Simulink environment was used for the simulations. The parameter values used in the controller were equal to those of the motor model. Fig. 5 shows results when the load torque was zero and the speed reference was changed stepwise from zero to 0.05 p.u. at $t = 1$ s., then reversed to -0.05 p.u. at $t = 2$ s., and finally set to zero at $t = 3$ s. Fig. 5(a) shows results when the minimum duration of the inverter voltage pulses was not limited, and Fig. 5(b) shows results when the duration was limited to 6 μ s. Although the system is stable in both cases, the effects of the distorted voltage can be clearly seen in Fig. 5(b). Voltage reference samples corresponding to the simulation in Fig. 5(b) are plotted in Fig. 6 separately for the lower and the upper zero voltage vector. The areas that do not have voltage reference samples correspond to the unallowable regions illustrated in Fig. 4. The minimum pulse limitation is enabled in the following simulations and experiments.

The phase currents and the d - and q -axis current components are shown in Figs. 7 and 8, respectively, corresponding to the simulation in Fig. 5(b). The HF current caused by the HF voltage signal is clearly visible in the figures. As can be seen in Fig. 7, the phase currents can be reliably estimated although only few samples are obtained in each period of the

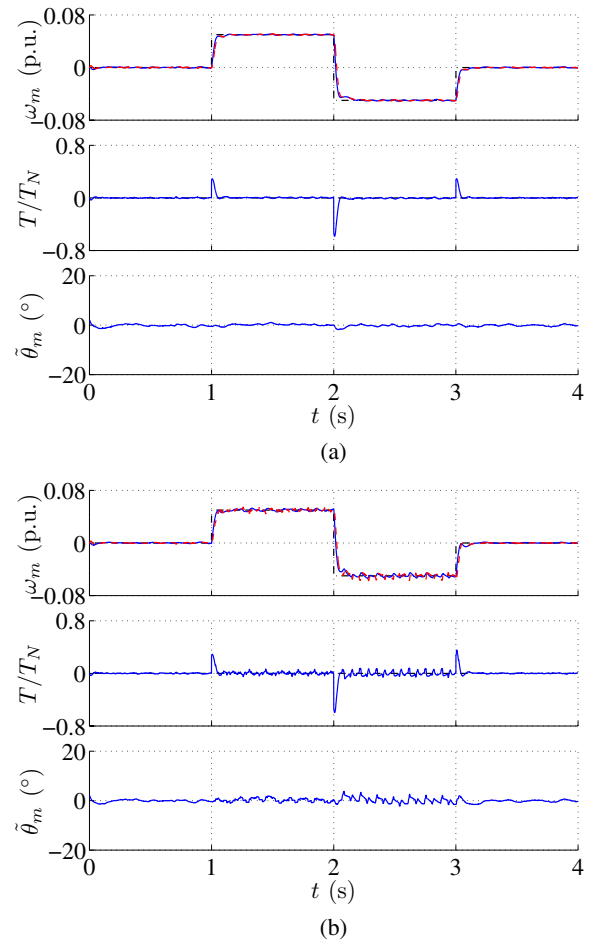


Fig. 5. Simulation results showing speed reference steps at no load: (a) minimum duration of voltage pulse not limited; (b) minimum duration of voltage pulse limited to 6 μ s. First subplot shows electrical angular speed (solid), its estimate (dashed), and its reference (dash-dotted). Second subplot shows estimated electromagnetic torque (solid) and load torque reference (dash-dotted). Last subplot shows estimation error of rotor position in electrical degrees.

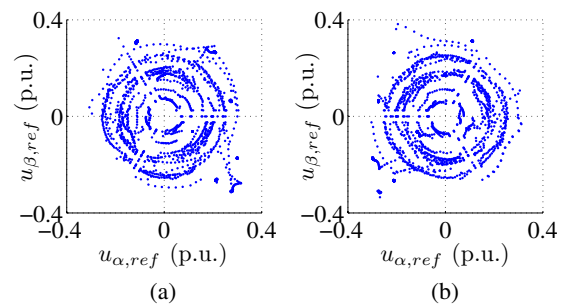


Fig. 6. Voltage references in the stator reference frame from the simulation in Fig. 5(b): (a) lower zero voltage vector; (b) upper zero voltage vector.

HF signal. Fig. 8 shows that the estimated and reconstructed currents follow the actual values well even during a transient state (speed reversal). The difference between the estimated and reconstructed d -axis current components is due to the current estimation error, which is commonly present during a transient. However, it is to be noted that the reconstructed currents follow the actual currents with good accuracy.

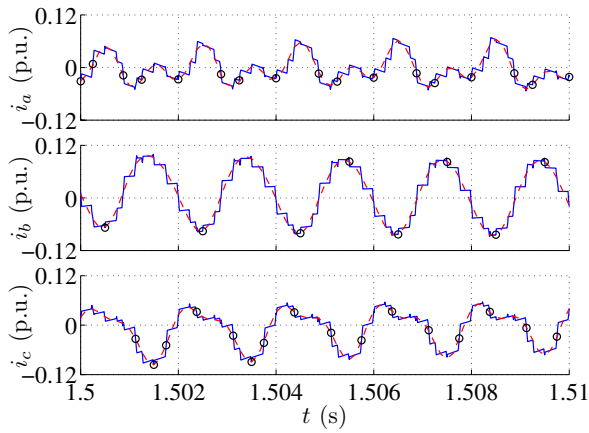


Fig. 7. Phase currents from the simulation in Fig. 5(b). First subplot shows phase a current, second subplot shows phase b current, and third subplot shows phase c current. Actual phase current is shown as solid line and reconstructed current as dashed line. The circles indicate samples obtained from the phase current.

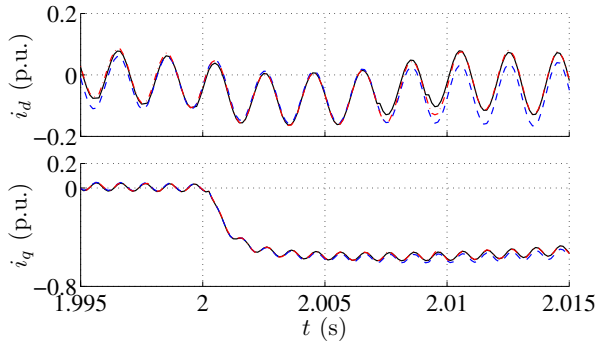


Fig. 8. Currents i_d and i_q from the simulation in Fig. 5(b). First subplot shows d -axis current, second subplot shows q -axis current. Phase currents converted to the estimated rotor reference frame are shown as solid line, estimated currents \hat{i}_d and \hat{i}_q as dashed line, and reconstructed currents $i_{d,dc}$ and $i_{q,dc}$ as dash-dotted line, which mostly overlaps the solid line.

Simulation results at zero speed reference are shown in Fig. 9. The load torque was changed stepwise from zero to the positive nominal value at $t = 1$ s, then reversed to the negative nominal value at $t = 2$ s, and finally set to zero at $t = 3$ s. The drive is stable, and the rotor position estimation error remains small, indicating good dynamic performance. Sustained operation at zero speed under load is also possible. Fig. 10 depicts simulation results during a slow speed reversal from $\omega_{m,ref} = 0.2$ p.u. to $\omega_{m,ref} = -0.2$ p.u. between $t = 1$ s and $t = 9$ s. The ripple visible in the curves is due to the stator voltage distortion caused by the minimum pulse limitation. In spite of the ripple, the system is stable in the speed reversal.

VI. EXPERIMENTAL RESULTS

The experimental setup is illustrated in Fig. 11. In the laboratory tests, the 2.2-kW PMSM described in Section V was fed by a commercial frequency converter with modified control software. Mechanical load is provided by a PMSM servo drive, and the actual rotor speed and position are monitored by an incremental encoder. The DC-link current is measured by a shunt resistor, and the control algorithms

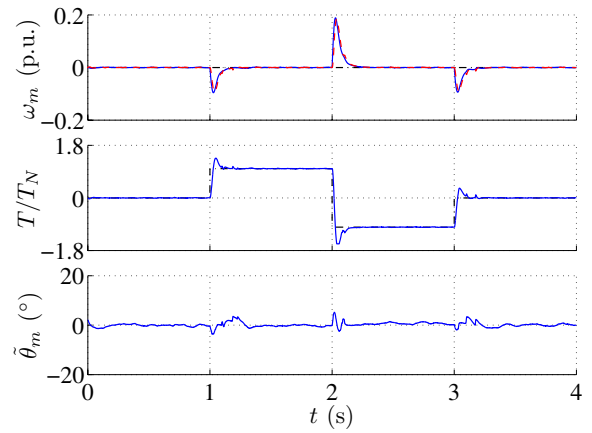


Fig. 9. Simulation results showing load torque steps at zero speed reference. Explanations of the curves are as in Fig. 5.

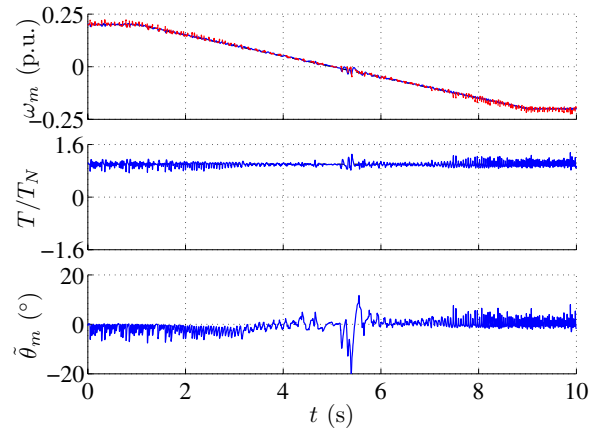


Fig. 10. Simulation results showing slow speed reversal at nominal load torque. Explanations of the curves are as in Fig. 5.

are implemented in a Texas Instruments TMS320F2811 DSP. The two-phase modulation scheme with synchronized current sampling is used. The commutation delays in the inverter bridge and the control delays of the IGBTs are compensated in a feedforward manner when calculating the switch turn references of the IGBTs. The minimum length of the voltage pulse in the beginning and in the middle of the switching period is limited to $6 \mu\text{s}$ in the modulator.

The nominal DC-link voltage is 540 V, the switching frequency 4 kHz, and the sampling frequency 8 kHz. In the experiments, the q -axis current reference was used to control the torque, and the d -axis current reference was set to zero. Due to practical restrictions, data could be captured from the control software to the computer only at an approximate rate of 15 samples in a second for each variable. An anti-aliasing filter having a bandwidth of 10 Hz was applied to the recorded variables. The actual rotor speed and position were monitored, and a faster transfer rate was used for these variables.

Fig. 12 shows experimental results under nominal load. The speed reference is changed stepwise from zero to 0.5 p.u. in steps of 0.125 p.u. Each step has a duration of 2 seconds. Finally, the speed reference is set to zero at $t = 10$ s. The system can cope with stepwise changes in the speed reference,

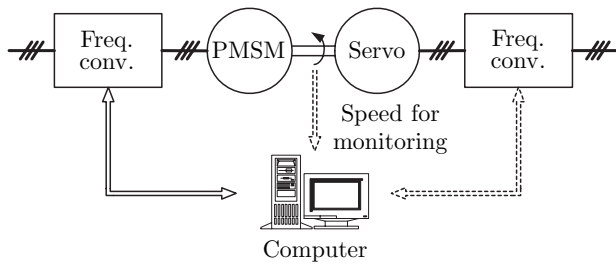


Fig. 11. Experimental setup. Mechanical load is provided by a servo drive.

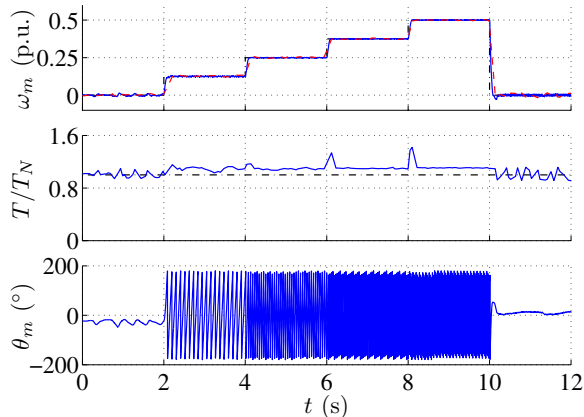


Fig. 12. Experimental results showing speed reference steps under nominal load torque. First subplot shows electrical angular speed (solid), its estimate (dashed), and its reference (dash-dotted). Second subplot shows estimated electromagnetic torque (solid) and load torque reference (dash-dotted). Last subplot shows true rotor position in electrical degrees.

and the operation is stable from zero speed to high speeds.

Experimental results showing nominal load torque steps at zero speed reference are depicted in Fig. 13. A positive load torque is applied between $t = 2$ s and $t = 4$ s, and a negative load torque is applied between $t = 6$ s and $t = 8$ s. The proposed method allows sustained operation at zero speed under nominal load, and is robust to fast load torque changes.

VII. CONCLUSIONS

The proposed method is suitable for vector control of PMSM drives when only the DC-link current is measured instead of the motor phase currents. A two-phase PWM method is used, allowing the phase currents to be sampled at uniform intervals. An adaptive observer is used for the estimation, and the current error used for feedback is updated using available phase current samples. The low-speed operation is stabilized by an HF signal injection method with a modified excitation voltage, and the adaptive observer is used for estimating the HF current response. The proposed method enables reliable estimation of the stator current, rotor speed, and rotor position, and is also insusceptible to the stator voltage distortion caused by the minimum pulse limitation. The simulation and experimental results presented in the paper show that the proposed method can operate in a wide speed range and can cope with transients in the speed reference and in the load torque.

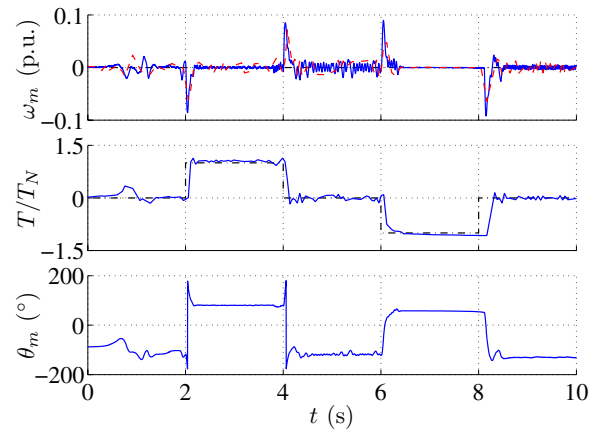


Fig. 13. Experimental results showing load torque steps at zero speed reference. Explanations of the curves are as in Fig. 12.

ACKNOWLEDGEMENT

The authors gratefully acknowledge the financial support given by ABB Oy, Walter Ahlström Foundation, and KAUTE Foundation.

REFERENCES

- [1] T. C. Green and B. W. Williams, "Derivation of motor line-current waveforms from the DC-link current of an inverter," *Proc. Inst. Elect. Eng. B*, vol. 136, no. 4, pp. 196–204, July 1989.
- [2] T. Habetler and D. M. Divan, "Control strategies for direct torque control using discrete pulse modulation," *IEEE Trans. Ind. Applicat.*, vol. 27, no. 5, pp. 893–901, Sept./Oct. 1991.
- [3] J. F. Moynihan, S. Bolognani, R. C. Kavanagh, M. G. Egan, and J. M. D. Murphy, "Single sensor current control of ac servodrives using digital signal processors," in *Proc. EPE'93*, vol. 4, Brighton, UK, Sept. 1993, pp. 415–421.
- [4] F. Blaabjerg, J. K. Pedersen, U. Jaeger, and P. Thøgersen, "Single current sensor technique in the DC link of three-phase PWM-VS inverters: a review and a novel solution," *IEEE Trans. Ind. Applicat.*, vol. 33, no. 5, pp. 1241–1253, Sept./Oct. 1997.
- [5] S. N. Vukosavic and A. M. Stankovic, "Sensorless induction motor drive with a single DC-link current sensor and instantaneous active and reactive power feedback," *IEEE Trans. Ind. Electron.*, vol. 48, no. 1, pp. 195–204, Feb. 2001.
- [6] U.-H. Rieder, M. Schroedl, and A. Ebner, "Sensorless control of an external rotor PMSM in the whole speed range including standstill using DC-link measurements only," in *Proc. IEEE PESC'04*, vol. 2, Aachen, Germany, June 2004, pp. 1280–1285.
- [7] H. Kim and T. M. Jahns, "Phase current reconstruction for AC motor drives using a DC link single current sensor and measurement voltage vectors," *IEEE Trans. Pow. Electron.*, vol. 21, no. 5, pp. 1413–1419, Sept. 2006.
- [8] M. Depenbrock, "Pulse width control of a 3-phase inverter with nonsinusoidal phase voltages," in *Proc. IEEE ISPC'77*, 1977, pp. 399–403.
- [9] S. Ogasawara, H. Akagi, and A. Nabae, "A novel PWM scheme of voltage source inverters based on space vector theory," in *Proc. EPE'89*, vol. 1, Aachen, Germany, Oct. 1989, pp. 1197–1202.
- [10] J. W. Kolar, H. Ertl, and F. C. Zach, "Influence of the modulation method on the conduction and switching losses of a PWM converter system," *IEEE Trans. Ind. Applicat.*, vol. 27, no. 6, pp. 1063–1075, Nov./Dec. 1991.
- [11] P. Virolainen, S. Heikkilä, and M. Hinkkanen, "Method for determining output currents of frequency converter," Finnish Patent *FI 116337 B*, Oct. 31, 2005.
- [12] A. Piippo, M. Hinkkanen, and J. Luomi, "Analysis of an adaptive observer for sensorless control of PMSM drives," in *Proc. IEEE IECON'05*, Raleigh, NC, Nov. 2005, pp. 1474–1479.
- [13] A. Piippo and J. Luomi, "Adaptive observer combined with HF signal injection for sensorless control of PMSM drives," in *Proc. IEEE IEMDC'05*, San Antonio, TX, May 2005, pp. 674–681.